Strain-accelerated HF etching of AlAs for epitaxial lift-off

2004 J. Phys.: Condens. Matter 16 3585

(http://iopscience.iop.org/0953-8984/16/21/008)

INSTITUTE OF PHYSICS PUBLISHING JOURNAL OF PHYSICS: CONDENSED MATTER

J. Phys.: Condens. Matter **16** (2004) 3585–3596 PII: S0953-8984(04)78185-0

Strain-accelerated HF etching of AlAs for epitaxial lift-off

M M A J Voncken[1], J J Schermer, G J Bauhuis, A T J van Niftrik and P K Larsen

Experimental Solid State Physics III, NSRIM, University of Nijmegen, Toernooiveld 1, 6525 ED Nijmegen, The Netherlands

E-mail: maartenv@sci.kun.nl

Received 17 March 2004
Published 14 May 2004
Online at stacks.iop.org/JPhysCM/16/3585
DOI: 10.1088/0953-8984/16/21/008

Abstract

Epitaxial lift-off (ELO) is a process which allows for the separation of a single crystalline III/V thin film or device from the substrate it was deposited on. This process is based on the selective etching of an intermediate AlAs release layer in an aqueous HF solution. The lateral etch rate of the AlAs release layer through a narrow crevice in the weight-induced epitaxial lift-off (WI-ELO) process is much larger than observed for unobstructed planar AlAs layers. It is possible that this increase in etch rate is caused by the tensile strain induced upon the AlAs layer in the WI-ELO setup. In order to verify this assumption, planar AlAs layers, subjected to a controlled curvature, were etched in HF solutions and their etch duration was measured. The applied curvature reduced the already present compressive strain due to lattice mismatch. For large applied bending radii no change in etch rate was observed, because the induced bending is smaller than the already present bending due to the lattice mismatch. Further bending induces a total compressive strain from -0.126% to -0.11%, resulting in an etch rate variation from 0.054 up to 0.066 mm h^{-1}. Measurements on AlAs layers experiencing a tensile strain of +0.286% showed much higher etch rates of 0.134 mm h^{-1}.

The present results obtained on etching experiments in the lateral plane are extrapolated to the perpendicular direction so that a combination with the data from previous work becomes feasible. This results in a better microscopic picture of the etch front in the WI-ELO process. It is found that the force exerted by the weight can be projected on an area, limited by the sample width and a depth of approximately 6 μm.

[1] Author to whom any correspondence should be addressed.

1. Introduction

The weight-induced epitaxial lift-off (WI-ELO) process is a technique which allows for the separation of a single crystalline film or device from the substrate it is deposited on [1, 2] (see figure 1). This is achieved by the selective chemical etching of an intermediate AlAs sacrificial layer with an aqueous HF solution. ELO can result in several benefits in device processing. The substrate remains unharmed and can therefore be reused, thereby reducing costs significantly. The lifted device is very thin, yielding multiple possibilities for applications that are not possible for devices on their substrate. A thin film III/V based opto-electronic device can for example be combined with a silicon based structure, thereby combining the benefits of both [3]. Thin film lasers can be mounted on excellent heat conductors like copper or diamond, so that larger power and heat dissipation becomes feasible. For solar cells, the cost reduction resulting from the substrate reuse is the most important drive for pursuing ELO research, although it should be noted that thin film solar cells offer some additional benefits as well. Recent work [4] has already shown that thin film solar cells reach efficiencies that are comparable and sometimes even better than those obtained for identical solar cell structures on a GaAs substrate. In concentrator setups, solar cells tend to become very hot; a thin film cell, which can be cooled more efficiently, is then an essential step towards higher concentration factors [5]. For space applications, where the weight of the solar cells is important, thin film cells with efficiencies comparable to cells on substrate are very desirable [6]. Finally, thin film solar cells show a much larger transparency for light with an energy that is smaller than the bandgap of the semiconductor material, compared to cells on their substrates. The thin film cells are therefore a more favourable candidate for the top cell in a mechanically stacked tandem solar cell [7]. Another application that utilizes a form of epitaxial lift-off is the fabrication of nanotubes or nanohelices [8–10]. A thin strained InGaAs/GaAs bilayer is separated from the GaAs substrate it is deposited on by the selective etching of a sacrificial AlAs layer with HF solution. Due to the intrinsic strain the bilayer curls up to form a perfect single-crystalline tube with a diameter varying between 2 nm and 100 μm and a wall thickness down to 0.5 nm [8]. Possible applications for these nanodevices include the formation of micro- and nanoneedles for biological applications [11] and for inkjet printing [12] and several other nanoelectronic and nanomechanic devices [13].

ELO is only suitable for large scale industrial utilization if the rate at which substrate and device are separated is high enough (i.e. comparable to the time that is needed for the crystal growth of the thin film structure). The lateral etch rate of the process as a function of the release layer thickness (h), temperature (T) and applied radius of curvature (R) of the film (see figure 1) has therefore been under serious investigation during recent years [2, 14–16]. Based on the generally used model as proposed by Yablonovitch *et al* [1], the maximum attainable etch rate $V_{\mathrm{e,max}}$ in an aqueous 10% HF solution as a function of the relevant process parameters would be given by

$$V_{\mathrm{e,max}} = \frac{0.23}{\sqrt{Rh}} \mathrm{e}^{-2551/T}, \tag{1}$$

with $V_{\mathrm{e,max}}$ in mm h^{-1}, R and h in mm and T in K [1, 2, 14]. Recent experiments, however, demonstrate that this model does not describe the process very well. For standard conditions ($R = 50$ mm, $h = 5$ nm and $T = 323$ K), the model predicts a lateral etch rate of 3 μm h^{-1}, whereas experiments already showed etch rates of the order of 5 mm h^{-1} under the same conditions [16]. Furthermore, a qualitative difference in the relation between $V_{\mathrm{e,max}}$ and R in the model and in experiments was found. Whereas the model predicts an inverse square root dependency of $V_{\mathrm{e,max}}$ on R, the experimental results obtained at $h = 5$ nm, $T = 323$ K and an

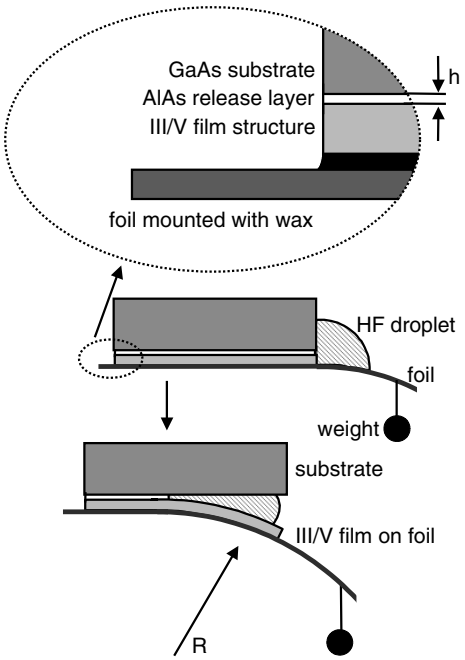

Figure 1. A schematic representation (cross section) of the WI-ELO setup. The relative size of the different parts is greatly out of proportion. The applied radius of curvature R is indicated.

HF concentration of 10% indicate a relation given by

$$V_e = 3.1 + 293R^{-1.2}, \tag{2}$$

with V_e in mm h^{-1} and R in mm [16]. This clearly shows that the relation between $V_{e,max}$ and R is not governed by an inverse square root, but by a more complicated connection. The first part of the right-hand side of equation (2) is a radius-independent part, which has been thoroughly investigated in earlier work [17], while the second part is radius dependent.

The radius-dependent part of equation (2) is under investigation in the present work. The most direct influence of a variation in the applied radius of curvature is a difference in the opening of the crevice and with this the exchange rate of reaction products. This, however, can never enhance the etch rate to values that exceed the bulk etch rate, as obtained for an unhampered etch process [16], by a factor of more than ten. The application of a force to the sample, however, also influences the material itself by placing it under tensile strain. In the present work, we describe the effects of strain on the etch rate of AlAs layers for planar samples subjected to a controlled curvature and for samples in the multi-release layer setup [17]. The results obtained are used to provide a better microscopic picture of the etch front in the WI-ELO setup.

2. Experimental details

All samples are grown using low pressure 'metal organic vapour phase epitaxy' (MOVPE) in a horizontal Aixtron 200 reactor. The source materials are trimethyl-gallium (TMGa) and trimethyl-aluminium (TMAl) for the group-III species and arsine (AsH_3) as the group-V species. Disilane (Si_2H_6) is used as a precursor material in order to obtain n-type doping. The carrier gas is hydrogen (total flow 6500 sccm) and the reactor pressure and temperature

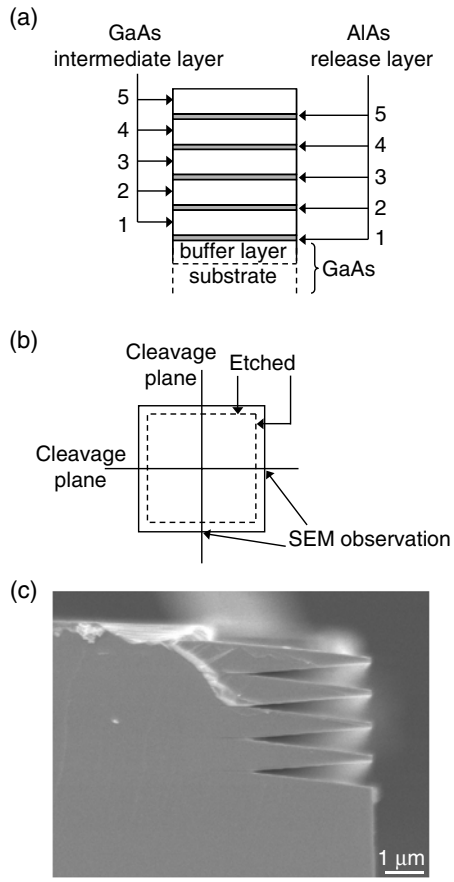

Figure 2. (a) Typical sample configuration, consisting of five identical GaAs layers of approximately 0.75 μm thickness, separated by AlAs release layers. (b) 1×1 cm^2 sample with lines along which it was cleaved. The cross-sections were observed with SEM. (c) SEM image of a cross-section, revealing the etched AlAs release layers. Due to the cleaving after etching, the top GaAs layer has broken off. It is clearly visible that by adding H_2O_2 to the HF etchant, the extreme etching selectivity of $\sim 10^6$ for AlAs over GaAs is lost.

are kept at 20 mbar and 650 °C, respectively. Two series of samples are produced: the first is for the experiments in which a controlled radius of curvature is applied, the second for a multi-release layer experiment, as described in previous work [17]. For the first series the substrates are 2 inch undoped (100) GaAs substrates, 2° off towards ⟨110⟩. The layer structure of the samples is given by a 0.3 μm thick undoped GaAs buffer layer, an n-type AlAs layer of 2 μm thickness and the samples are topped with a 150 nm thick undoped GaAs cap layer in order to prevent premature oxidation of the AlAs layer. For the second series the substrates are 2 inch n-type GaAs substrates with identical crystal orientation. The layer structure is given by a 0.3 μm thick n-type GaAs buffer layer, followed by a stack of 5 n-type AlAs layers of 10 nm thickness, sandwiched between 5 n-type GaAs intermediate layers of 0.75 μm thickness (see figure 2(a)), identical to the calibration sample in previous work on the multi-release layer experiments [17].

The first objective of the present study is to apply controlled curvature to the samples and measure the AlAs etch rate in an aqueous HF solution as a function of the thus induced strain in the layer. Because the originally 350 μm thick GaAs wafers only allow a relatively

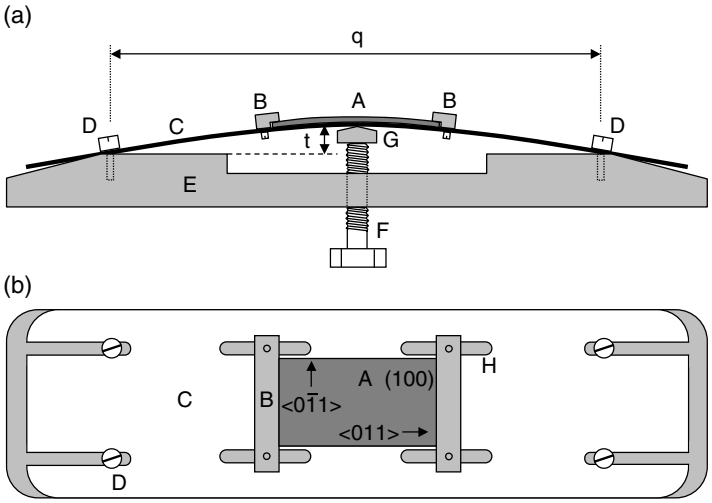

Figure 3. (a) Side view and (b) top view of the plastic device used to induce a curvature to the samples during etching (the bender). The sample (A) (crystal orientations are indicated) is secured on a flexible plate (C) with two holders (B). The flexible plate is attached to the base plate (E) with four nylon screws (D) separated by a distance q. A large nylon screw (F) is used to raise a rigid bar (G), which pushes the top plate upwards over a distance t, resulting in a certain radius of curvature of the top plate. The bar is used to ensure that the curvature of the top plate and thus that of the sample is two-dimensional. The holes for screws (D) in the top plate are elongated to allow for this curvature. The holes (H) for the screws in (B) are also elongated to facilitate a secure clamping of the sample to the top plate.

small bending ($r > 250$ mm, with r the induced radius of curvature due to bending) before the samples break, the samples are first thinned by a chemical etch process. For this purpose the wafers are cleaved into samples of approximately 10×15 mm^2. The front sides of the samples are then covered with black wax (Apiezon) and the samples are etched from the backside with a citric acid–hydrogen peroxide solution (5:1) for 14 h 42 min. At an average etch rate of 0.34 μm min^{-1}, this results in samples with a GaAs substrate thickness of 50 μm. Radii of curvature down to 80 mm are then attainable without breaking the samples.

After the thinning procedure, the samples are cleaned by dissolving the wax with trichloroethylene and mounted on a device (the bender), which is able to provide the sample with the desired radius of curvature (see figure 3). The sample is fixed on a flexible plate with two holders and the plate is mounted on a base-plate with nylon screws. A large screw in the base-plate is used to apply a controlled curvature to the flexible plate, thereby applying the same curvature to the sample. The entire bender is made of plastic (Pertinax base-plate, polypropylene flexible top-plate and nylon screws) for chemical stability and to ensure that the etch process is not influenced by other chemical reactions.

The samples are mounted while the flexible plate is straight. Then the bender is immersed in an ammonia–peroxide (NH_3:H_2O_2:H_2O = 2:1:10) etching solution in order to remove the GaAs cap layer. Preliminary experiments showed that the GaAs etch rate in this solution is 1.11 μm min^{-1}, so the 150 nm thick cap layer is removed in approximately 8 s. To ensure that the cap layer is removed completely, an etch duration of 30 s is chosen. However, it should be noted that in the additional time the AlAs layer is already slightly attacked. The rate at which this occurs was measured to be 0.05 μm min^{-1}, so that the effective AlAs layer thickness is only reduced by about 1%, which is well within the error margins of these experiments. Immediately after the cap etch the bender with mounted sample is transferred to a large beaker

with nanopure water and thoroughly rinsed. While keeping the bender immersed in the water, the desired radius of curvature is applied to the sample via screw F (see figure 3). Values for t are chosen between 0 and 7 mm, resulting in radii of curvature varying between infinity and 80 mm. The samples were found to break if a smaller radius is applied. Subsequently the bender is immersed in the actual etchant: aqueous HF solution. The HF solution is stirred to avoid possible diffusion problems during the etch process. By a change of colour, it is clearly visible when the AlAs layer is completely etched away, thereby revealing the underlying GaAs. The time needed for etching through the AlAs layer is measured, thereby yielding the etch rate. In order to minimize measurement errors, a long etch duration is favoured. This would suggest choosing a low HF concentration. Experiments, however, showed that if the HF concentration is chosen below 10%, the etch process is not very reproducible, because in some cases a black debris is formed on the samples. Logan *et al* also found this debris and they referred to it as glassy oxides [18]. These oxides prevent the etch process from progressing, or suddenly detach and show a completely etched AlAs layer. At HF concentrations of 10% and higher, the etch process progresses reproducibly, but the etch times are only ∼5 s. This does not allow for an accurate time measurement. The solution to the problem was found by the use of an HF solution with a low concentration (0.5%) combined with H_2O_2 (HF (48%):H_2O_2 (30%):H_2O = 5:24:451). Etching in this solution proved to be reproducible, and no stabilizing oxides or glasses are formed. In the rest of this work it is assumed that the rate limiting step in the etching process is the same for etching with aqueous HF or with aqueous HF/H_2O_2 solution. If this step, however, is different, it does not influence the general conclusions of the present work. The etch times are around 2 min, which makes accurate timing possible. Three times were measured, the first when the first spot of GaAs becomes visible through the etched AlAs layer, the second when the AlAs layer is removed over about half the area of the sample, and the third when the entire AlAs layer has disappeared. Since the first etch time is not very reproducible, the etch time was calculated by averaging the second and third measured etching time. A series with values of t varying between 0 and 7 mm was performed twice and the results were averaged.

The second objective is to measure the AlAs etch rate in the multi-release layer setup. The samples of the second series are cleaved in pieces of approximately 1×1 cm^2 and etched for 2 min in the same HF–H_2O_2–H_2O mixture as used in the first series. After etching, the samples are thoroughly rinsed in nanopure water for 10 min and subsequently delicately blown dry with nitrogen. The samples are then cleaved into four pieces and the cross-sections are examined with scanning electron microscopy (SEM) (see figure 2(b)). The SEM images show how deep each AlAs layer has etched in 2 min, thereby revealing the etch rate, as shown in figure 2(c). A detailed description of the multi-release layer technique is given in previous work [17]. Twelve samples were measured by SEM, leading to 60 data-points (5 AlAs layers per sample), which are corrected for the position in the sample and for the GaAs etch rate. According to the established procedures [17] averaging them leads to a representative value for the etch rate.

It should be noted that in the first series of experiments the compressive strain is in the x–y-direction (in plane with the surface of the substrate), while the AlAs layers are etched in the z-direction (perpendicular to the substrate). In the multi-release layer setup, however, the tensile strain is in the z-direction, while the etching occurs in the x- and y-directions.

3. Results and discussion

3.1. Strain in AlAs layers

The applied distance t in the experiments is used to calculate the radius of curvature r of the sample. The distance q between the two sets of flexible screws (D) at the left-hand and

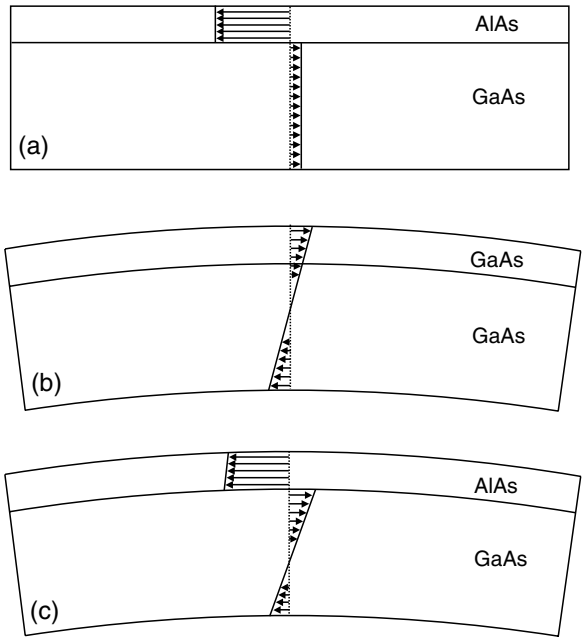

Figure 4. Compressive (arrows to the left) and tensile (arrows to the right) strains in a substrate plus epilayer. (a) Situation where the lattice mismatch strain is equally distributed over the thickness of the substrate and the epilayer. Note that the substrate is generally much thicker than the epilayer, so that the strain in the substrate can be neglected. (b) Strain distribution in a bent sample without lattice mismatch. (c) Strain distribution in a bent sample with lattice mismatch, which is a superposition of both previous situations. Note that samples with a lattice mismatch between epilayer and substrate show spontaneous bending to a certain curvature (i.e. without exerting an external force).

right-hand side in figure 3 is fixed at 65 mm. For small values of t, r is then found by assuming a circular shape of the flexible top plate:

$$r = \frac{t^2 + (q/2)^2}{2t}, \tag{3}$$

with r, t and q in mm. The strain in the AlAs film ε is defined as $\varepsilon = \Delta L/L_0$ with L_0 the sample length without stress and ΔL the induced extra length. The plate (substrate plus film) is clamped and it is assumed that the sample length in the mid-plane is unchanged by the bending. This means that the upper half of the substrate plus film is under tensile strain and the bottom half is under compressive strain (see figure 4(b)). Via

$$\frac{L_0}{r} = \frac{\Delta L}{d/2}, \tag{4}$$

with d the thickness of substrate plus film, it follows that ε is given by

$$\varepsilon = \frac{d}{2r}. \tag{5}$$

The stress σ is usually calculated via $\sigma = \varepsilon E$ with E the Young's modulus. The Young's modulus is strongly dependent on the crystal orientation of the samples. Furthermore, a correction for bi-axial stresses is generally applied by replacing E with $E/(1-\nu)$, with ν the Poisson ratio. This Poisson ratio is also crystal orientation dependent, varying between 0.33 and 0.024 for different crystal orientations. In the present study, samples with crystal

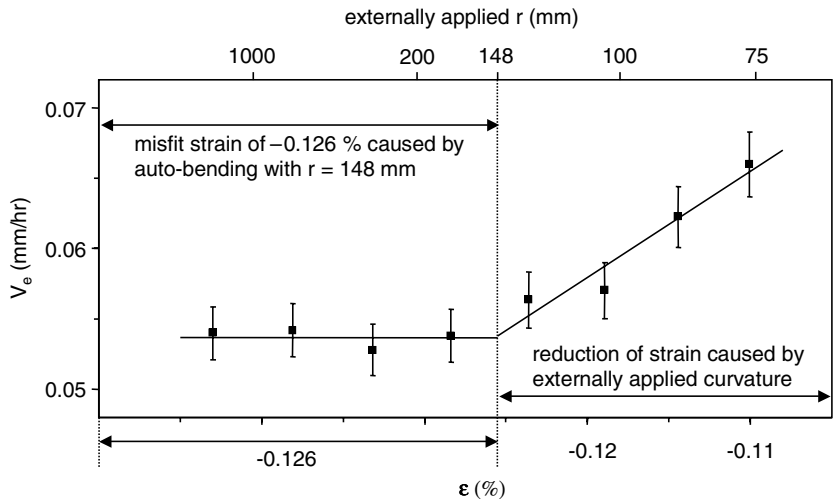

Figure 5. The etch rate of AlAs under reduced compressive strain in an 0.5% aqueous HF/H_2O_2 solution. The width of the error bars is given by ±3.5%, which was estimated from the timing errors in the etching experiments. The top horizontal axis denotes the externally applied radius of curvature r. The vertical dotted line indicates the point at which the externally applied bending equals the bending induced by the lattice mismatch. Left of the dotted line the strain in the AlAs layer is equal to −0.126%. This is a reduction of the 0.143% from the lattice mismatch, due to the auto-bending of the sample.

orientations in the (100) plane are used; the stress is in the $\langle 011 \rangle$ direction, while the transverse strain is in the $\langle 0\bar{1}1 \rangle$ direction. The values for E (120 GPa for AlAs and 122 GPa for GaAs) and ν (0.024 for both) are almost identical in this case [19]. In further calculations E_{AlAs} is set equal to E_{GaAs}, an approximation that is justified by their small differences and the fact that the substrate plus epilayer consists for ∼96% of GaAs. Furthermore, ν is set equal to zero, because the bi-axial stress effects are very small, i.e. $\nu \ll 1$. By combining equations (3) and (5) the resulting strain is directly related to the distance t of the bender:

$$\varepsilon = \frac{td}{t^2 + (q/2)^2}. \tag{6}$$

AlAs has a slightly larger lattice constant, compared to GaAs (0.566 139 nm for AlAs versus 0.565 330 nm for GaAs at room temperature [19]), resulting in a compressive strain of $\varepsilon = -0.143\%$ and an associated stress of $\sigma = -0.174$ GPa. The tensile strain that is applied by bending the samples is added to the compressive strain that is already present in the epilayer (see figure 4). From equation (6) it follows that for $d = 50$ μm and the largest possible t of 7 mm, a tensile strain of +0.0317% is reached, so the compressive strain in the layer, due to the lattice mismatch, is about five times larger than the maximum inducible tensile strain due to sample bending. Bending therefore leads to a reduction of the compressive strain. In the present experiments the influence of this reduced compressive strain on the etch rate has been measured.

The results of these experiments are given in figure 5. It is clearly visible that for little bending (externally applied radius of curvature $r > \sim 150$ mm) no visible effect is found. This can be explained by the fact that the GaAs–AlAs stack is already curved due to the intrinsic lattice mismatch. This curvature is not undone by clamping the sample to the flexible top plate.

The curvature can be calculated using the Stoney formula [20]:

$$\sigma_f = \frac{1}{6r}\frac{E_s d_s^2}{(1-\nu_s)d_f}, \tag{7}$$

where the index s refers to substrate (GaAs) and f to film (AlAs). For the previously calculated stress, a value for r of 148 mm follows, which is in excellent agreement with the experimentally determined value of ∼150 mm. This value is reached when t equals 3.6 mm. The extra bending of the sample therefore only influences the system when t is larger than 3.6 mm. This corresponds well with the results obtained in figure 5. For values of t exceeding 3.6 mm a clear effect of the bending and thus reduced compressive strain on the etch rate is observed. A linear fit through these data points is given by

$$V_e = 0.15 + 75.5\varepsilon, \tag{8}$$

with V_e the etch rate in mm h^{-1}.

The experiments with the multi-release layer samples show an averaged etch rate of 0.134 mm h^{-1}. This etch rate was obtained for the etching of AlAs under tensile strain, sandwiched between two GaAs layers. The magnitude of the tensile strain can be calculated from the fact that the volume of a unit cell of AlAs remains constant, so a compression of −0.143% (lattice mismatch) in two directions leads to a tensile strain of +0.286% in the perpendicular direction (σ = +0.343 GPa). From this result it already becomes clear that strain has a large influence on the etch rate. AlAs layers under tensile strain etch approximately 2.5 times faster than planar AlAs layers, which experience compressive strain for the aforementioned values of ε. However, the measured value of 0.134 mm h^{-1} is significantly lower than the value predicted by equation (8) (0.366 mm h^{-1}). This could be due to the fact that in the multi-release layer setup the etch process takes place through a narrow etch crevice, without any applied radius of curvature to facilitate the exchange of etchant and reaction products, while the etch process described by equation (8) is characterized by a free and unhampered exchange of etchant and reaction products.

3.2. Relation with the WI-ELO process

Both the etching experiments on planar AlAs layers and on the multi-release layers show that an increase in the AlAs etch rate occurs if the bonds between the atoms increase in length, i.e. if a layer is experiencing a positive difference in strain. In the WI-ELO process, a positive difference in strain is also present, as shown in figure 6. Instead of a reduction of the compressive strain, now an increase of tensile strain is encountered. If we assume that the relation between strain and change in etch rate is similar for both compressive and tensile strains, it becomes possible to obtain a better description of the ELO etching process on a microscopic scale. In the first place it becomes possible to elaborate in more detail the assumption made in previous work [16] that the differences in etch rate as a function of the radius of curvature in the WI-ELO configuration (see figure 1) are related to strain in the release layer. In the second place it allows for an estimation of the release layer area on which the force applied by the weight in the WI-ELO configuration actually works (see figure 6).

It was found that the lateral etch rate as a function of the applied ELO radius of curvature R is given by equation (2). Because in this equation the etch rate of 3.1 mm h^{-1} is considered to be the radius-independent part, the increase in etch rate, as a function of this R, is defined via the factor f:

$$f = \frac{3.1 + 293R^{-1.2}}{3.1}. \tag{9}$$

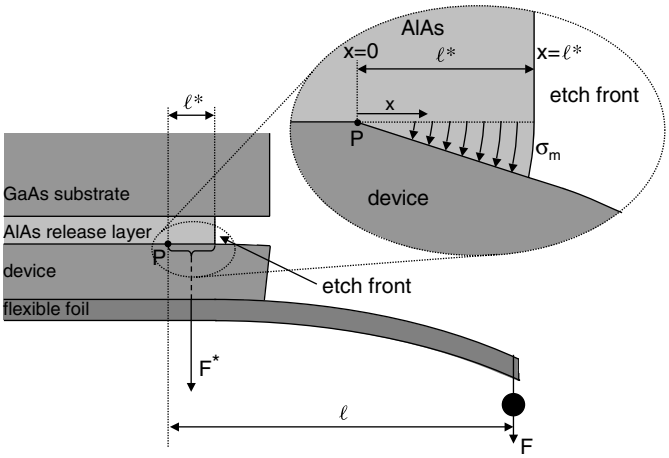

Figure 6. Detail of figure 1 giving a schematic representation (cross-section) of the strain in the AlAs release layer during etching in the WI-ELO configuration. In this approach the strain in the z-direction increases from the previously calculated +0.343 GPa up to σ_m from a certain point P towards the etch front. The width of the sample (b), i.e. perpendicular to the plane of paper, is typically 15 mm.

A similar factor f' can be deduced from figure 5, which correlates the factor to the strain in the layer:

$$f' = \frac{0.15 + 75.5\varepsilon}{0.15}. \tag{10}$$

In the previous work [16] factors f varying between 1 and 10 were found for R varying between infinity and 7 mm. For these factors, an estimate of the increase in strain can be made if we assume that the increase in etch rate can be fully attributed to strain in the layers. The AlAs layer, which is sandwiched between two GaAs layers, is compressively strained in the directions parallel to the GaAs substrate surface, and consequently under tensile strain perpendicular to this surface with an ε of +0.286%. Equation (10) then shows that the increase in etch rate with respect to an unstrained layer is already a factor 2.45. A further increase in etch rate by a factor of 10 (maximum observed) yields an ε of 4.63%. Although this looks like a very large value for ε, lengthening of interatomic bonds by this value is not extreme. In chemical reactions, for example, stretching of bonds by ~5% is not uncommon [21–23]. From this strain, the maximum stress (σ_m) at the etch front is calculated to be 5.6 GPa via $\sigma_m = \varepsilon E$.

As shown in figure 6, the force that the weight exerts on the AlAs release layer can be projected on a small area near the etch front, given by the sample width (b) times a certain depth (ℓ^*). This force depth ℓ^* on which the force due to the applied weight actually works can be estimated using the relation, described in equation (8), combined with results obtained in previous work [16]. In order to calculate the distance ℓ^* from P to the etch front, the force applied by the weight on the foil, given by $m \cdot g$, is projected as a force F^*, acting on the area (A) limited by b and ℓ^*, using a line through point P as the axis of rotation (see the magnified detail in figure 6). In this situation the moments M and M^* of F and F^*, respectively, with respect to P should be equal. The distance between the weight and point P is given by ℓ, so this moment is described by $M = F \cdot \ell = mg\ell$. F^* is calculated from $F^* = \sigma A$, resulting in

$$F^* = \int_{x=0}^{\ell^*} \sigma_m b \frac{x}{\ell^*} \, \mathrm{d}x, \tag{11}$$

with x the distance from point P towards the etch front. The moment is then given by

$$M^* = \int_{x=0}^{\ell^*} \sigma_m b \frac{x}{\ell^*} x \, dx = \frac{\sigma_m b \ell^{*2}}{3}. \tag{12}$$

By equating both moments, ℓ^* is calculated to be

$$\ell^* = \sqrt{\frac{3mg\ell}{\sigma_m b}}. \tag{13}$$

For realistic values of these parameters, such as $m = 5$ g, $\ell = 2$ cm and $b = 15$ mm, as used in previous work [16], the distance ℓ^* is estimated to be 6 μm. This indicates that all forces exerted by the weight on the foil are projected on an area that is only a few microns deep. The value of σ_m is calculated from an extrapolation of the measured data, shown in figure 5. The experiments with the multi-release layers already showed a difference in etch rate between the extrapolated value and the actually measured value by a factor of $\sim$2.5. For the multi-release layer setup, a predicted etch rate of 0.366 mm h^{-1} finally resulted in an actual etch rate of 0.134 mm h^{-1}; the difference is attributed to both measurement errors and to hampering of the etch process through a narrow etch crevice. This indicates that the actual σ_m during the WI-ELO process might be as much as 2.5 times larger than the one used in these calculations. In that case, the value of ℓ^* would be given by 4 μm.

4. Conclusions

In the WI-ELO etch process the lateral etch rate that is obtained when etching AlAs with HF solution through a narrow crevice is much larger than the etch rate obtained in etching planar AlAs layers without any obstructions. In previous work it was suggested that this effect might be due to applied stress to the AlAs layers. In the present work, it has been investigated whether or not the etch rate is influenced by strain differences in AlAs epitaxial films. AlAs layers on GaAs are already under compressive strain due to a lattice mismatch. A controlled reduction of this compressive strain can be induced by bending a thinned GaAs substrate with an AlAs epilayer. For applied bending radii between infinity and 148 mm, no change in etch rate was observed, because the applied bending is smaller than the intrinsic bending of the wafer due to the lattice mismatch. Further bending with radii of curvature from 148 mm down to 79 mm induces a change of the strain at the surface of the AlAs film ranging from -0.126% up to -0.11%. Under these conditions a positive influence on the etch rate was found, which can be described by $V_e = 0.15 + 75.5\varepsilon$ with V_e the etch rate in mm h^{-1}. Based on this relation an etch rate of 0.366 mm h^{-1} is expected for AlAs layers under tensile strain in the cross-section of multi-release layer samples. Experimentally, however, an etch rate of only 0.134 mm h^{-1} was found for these AlAs layers. The difference could be due to the hampering of a free exchange of etchant and reaction products. However, it should be noted that the etch rate for layers under tensile strain is significantly higher than that for compressively strained layers (by a factor 2.5). Based on the positive correlation found between strain and etch rate in the etching of planar AlAs layers, and the difference between the etch rate for layers under compressive and tensile strain, it becomes plausible to assume that a positive difference in the strain in the AlAs layer can result in a significant increase in the etch rate.

By combining previous work [16] with the present results, it became feasible to obtain a better microscopic picture of the etch front. In the previous work, the increase in etch rate, related to an applied radius of curvature, was already revealed. The present work revealed the relation between a positive change in strain and the increase in etch rate. By combining these two results the magnitude of the stressed region in the AlAs layer could be estimated. It

was found that all forces originating from the weight that induces the radius of curvature are projected on an area limited by the sample width and a depth of approximately 4–6 μm.

References

[1] Yablonovitch E, Gmitter T, Harbison J P and Bhat R 1987 *Appl. Phys. Lett.* **51** 2222–4
[2] Schermer J J, Bauhuis G J, Mulder P, Meulemeesters W J, Haverkamp E, Voncken M M A J and Larsen P K 2000 *Appl. Phys. Lett.* **76** 2131–3
[3] Ersen A, Schnitzer I, Yablonovitch E and Gmitter T 1993 *Solid-State Electron.* **36** 1731–9
[4] Bauhuis G J, Schermer J J, Mulder P, Voncken M M A J and Larsen P K 2004 *Sol. Energy Mater. Sol. Cells* at press
[5] Feteha M Y and Eldallal G M 2003 *Renew. Energ.* **28** 1097–104
[6] Lisbona E F, Signorini C and Bogus K P 2001 *Sol. Energy Mater. Sol. Cells* **66** 487–94
[7] Bett A W, Adelhelm R, Agert C, Beckert R, Dimroth F and Schubert U 2001 *Sol. Energy Mater. Sol. Cells* **66** 541–50
[8] Prinz V Y, Seleznev V A, Gutakovsky A K, Chehovskiy A V, Preobrazhenskii V V, Putyato M A and Gavrilova T A 2000 *Physica* E **6** 828–31
[9] Prinz V Y, Chehovskiy A V, Preobrazhenskii V V, Semyagin B R and Gutakovsky A K 2002 *Nanotechnology* **13** 231–3
[10] Deneke C, Müller C, Jin-Phillipp N Y and Schmidt O G 2002 *Semicond. Sci. Technol.* **17** 1278–81
[11] Prinz A V and Prinz V Y 2003 *Surf. Sci.* **532–535** 911–5
[12] Prinz A V, Prinz V Y and Seleznev V A 2003 *Microelectron. Eng.* **67/68** 782–8
[13] Prinz V Y 2003 *Microelectron. Eng.* **69** 466–75
[14] Maeda J, Sasaki Y, Dietz N, Shibahara K, Yokoyama S, Miyazaki S and Hirose M 1997 *Japan. J. Appl. Phys.* 1 **36** 1554–7
[15] Sasaki Y, Katayama T, Koishi T, Shibahara K, Yokoyama Y, Miyazaki S and Hirose M 1999 *J. Electrochem. Soc.* **146** 710–2
[16] Voncken M M A J, Schermer J J, Maduro G, Bauhuis G J, Mulder P and Larsen P K 2002 *Mater. Sci. Eng.* B **95** 242–8
[17] Voncken M M A J, Schermer J J, Bauhuis G J, Mulder P and Larsen P K 2004 *Appl. Phys.* A at press
[18] Logan R A and Reinhart F K 1973 *J. Appl. Phys.* **44** 4172–6
[19] Adachi S (ed) 1993 *Properties of Aluminium Gallium Arsenide* (*EMIS Datareviews Series No. 7*) (London: INSPEC) p 24
[20] Ohring M 1992 *The Materials Science of Thin Films* (San Diego, CA: Academic) p 418
[21] Ku Kang J and Musgrave C B 2002 *J. Chem. Phys.* **116** 275–80
[22] Sayle D C 1998 *J. Mater. Chem.* **9** 607–16
[23] Sayle D C, Maicaneanu S A, Slater B and Catlow C R A 1999 *J. Mater. Chem.* **9** 2779–87